European Journal of Radiology 175 (2024) 111426

Contents lists available at ScienceDirect

European Journal of Radiology

journal homepage: www.elsevier.com/locate/ejrad

Research article

Qualitative and quantitative image quality of coronary CT angiography using photon-counting computed tomography: Standard and Ultra-high resolution protocols

Borbála Vattay [a], Melinda Boussoussou [a], Milán Vecsey-Nagy [a], Márton Kolossváry [b,c], Dénes Juhász [a], Nóra Kerkovits [d], Hanna Balogh [d], Norbert Nagy [d], Miklós Vértes [d], Máté Kiss [e], Anikó Kubovje [d], Béla Merkely [a], Pál Maurovich Horvat [d], Bálint Szilveszter [a,*]

[a] Heart and Vascular Center, Semmelweis University, 1122 Budapest, Városmajor Street 68., Hungary
[b] Gottsegen National Cardiovascular Center, 29 Haller Utca, 1096, Budapest, Hungary
[c] Physiological Controls Research Center, University Research and Innovation Center, Óbuda University, Bécsi Ut 96/B, 1034, Budapest, Hungary
[d] Medical Imaging Center, Semmelweis University, 1082 Budapest, Korányi Sándor Street 2., Hungary
[e] Siemens Healthcare GmbH, Forchheim, Germany

ARTICLE INFO

Keywords:
Computed Tomography Angiography
Coronary CTA
Coronary Stents
Image Quality

ABSTRACT

Purpose: We aimed to identify the optimal reconstruction settings based on qualitative and quantitative image quality parameters on standard and ultra-high resolution (UHR) images using photon-counting CT (PCCT).
Method: We analysed 45 patients, 29 with standard and 16 with UHR acquisition, applying both smoother and sharper kernel settings. Coronary CT angiography images were performed on a dual-source PCCT system using standard (0.4/0.6 mm slice thickness, Bv40/Bv44 kernels, QIR levels 0–4) or UHR acquisition (0.2/0.4 mm slice thickness, Bv44/Bv56 kernels, QIR levels 0–4). Qualitative image quality was assessed using a 4-point Likert scale. Image noise (SD), signal-to-noise ratio (SNR) and contrast-to-noise ratio (CNR) were calculated in both the proximal and distal segments.
Results: On standard resolution, larger slice thickness resulted in an average increase of 12.5 % in CNR, whereas sharper kernel led to an average 8.7 % decrease in CNR. Highest CNR was measured on 0.6 mm, Bv40, QIR4 images and lowest on 0.4 mm, Bv44, QIR0 images: 25.8 ± 4.1vs.8.3 ± 1.6 ($p < 0.001$). On UHR images, highest CNR was observed on 0.4 mm, Bv40, QIR4 and lowest on 0.2 mm, Bv56 and QIR0 images: 21.5 ± 3.9vs.3.6 ± 0.8 ($p < 0.001$). Highest qualitative image quality was found on images with Bv44 kernel and QIR level 3/4 with both slice thicknesses on standard reconstruction. Additionally, Bv56 with QIR4 on 0.2 mm slice thickness images showed highest subjective image quality. Preserved distal vessel visualization was detected using QIR 2–4, Bv56 and 0.2 mm slice thickness.
Conclusions: Photon-counting CT demonstrated high qualitative and quantitative image quality for the assessment of coronaries and stents.

1. Introduction

Coronary CT angiography (CTA) has emerged as the first line diagnostic method for the detection of coronary artery disease (CAD) in low- and intermediate-risk chronic coronary syndrome patients [1]. Despite its widespread utilization, the evaluation of coronary stenosis in the presence of extensive calcification and coronary stents is limited when using conventional energy-integrating detector CT (EID-CT) scanners. Blooming artifact caused by heavy calcification can lead to the overestimation of luminal stenosis while a metal artifact caused by coronary stents could hinder the ability to assess stent patency and restenosis [2].

In recent years, novel photon-counting CT (PCCT) has been

Abbreviations: CAD, Coronary artery disease; CNR, Contrast-to-noise ratio; CTA, Computed tomography angiography; EID-CT, Energy-integrating detector computed tomography; HU, Hounsfield unit; LAD, Left anterior descending; LCX, Left circumflex; UHR, Ultra-high resolution; PCCT, Photon-counting computed tomography; QIR, Quantum iterative reconstruction; RCA, Right coronary artery; ROI, Region of interest; SD, Standard deviation; SNR, Signal-to-noise ratio.

* Corresponding author at: 18 Határőr út, 1122, Budapest, Hungary
E-mail address: szilveszter.balint@med.semmelweis-univ.hu (B. Szilveszter).

https://doi.org/10.1016/j.ejrad.2024.111426
Received 5 October 2023; Received in revised form 13 February 2024; Accepted 11 March 2024
Available online 12 March 2024

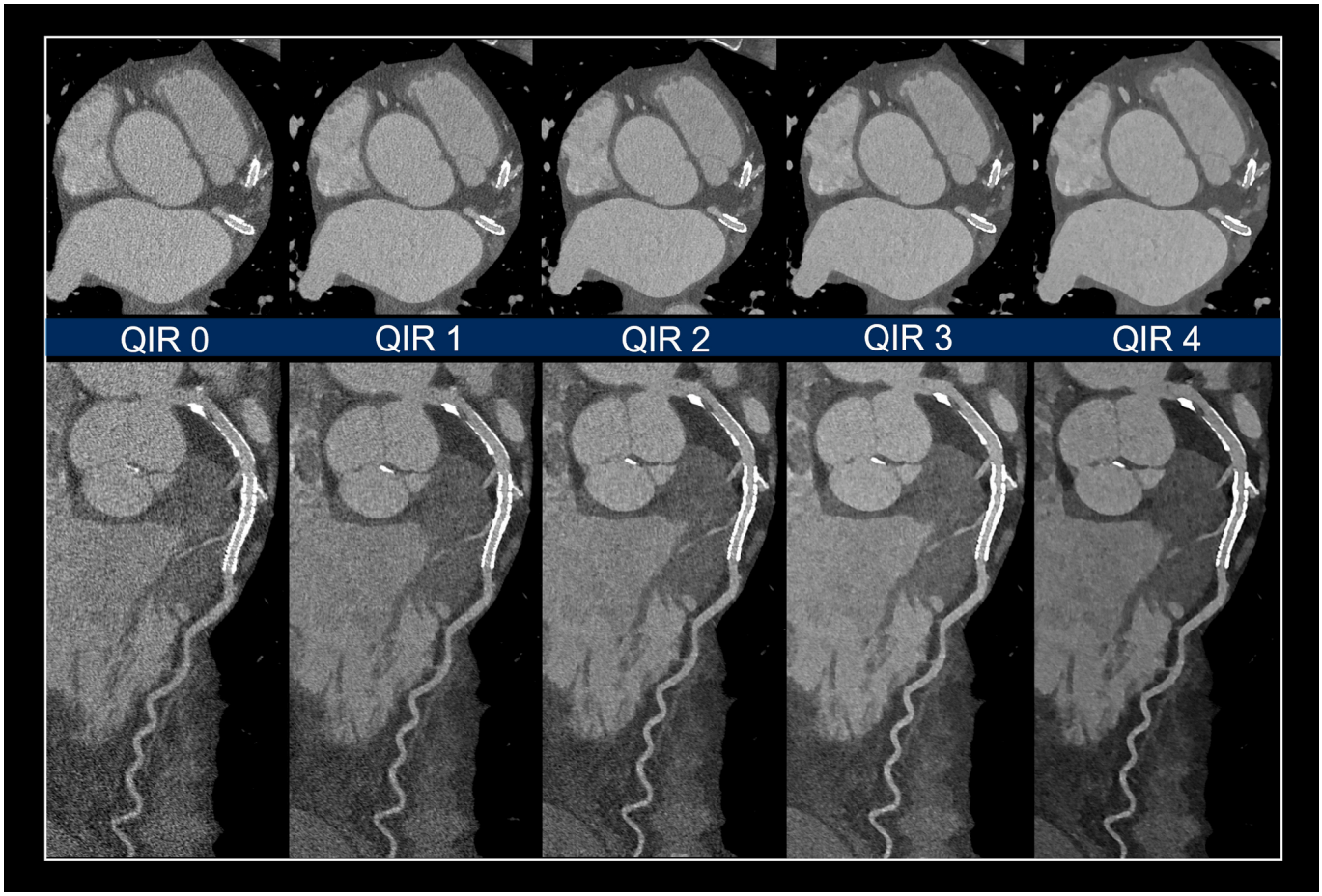

Fig. 1. Representative CTA images of coronary stents using UHR acquisition mode reconstructed using 0.2 mm slice thickness and sharp convolution kernel dedicated for vascular imaging (Bv56) with different strength levels of iterative reconstruction (QIR 0–4).

developed utilizing an innovative detector technology [3]. Photon-counting detectors register and convert each x-ray photons directly to electrical signal proportional to the energy of the incoming photon, allowing for spectral imaging, artifact reduction and reduced electronic noise [4]. The detectors are made of semiconductors containing smaller detector elements maintaining optimized geometric dose efficiency without the need of separating layers, resulting in improved spatial resolution [3]. The recently introduced dual-source PCCT scanner acquires spectral coronary CTA imaging with a slice thickness of 0.4 mm and enables ultra-high-resolution (UHR) scan mode with a slice thickness of 0.2 mm without dose penalty [5]. Quantum iterative reconstruction (QIR) algorithm has been developed to counterbalance the increased noise of high-resolution imaging. Previous studies have demonstrated improved image quality of PCCT for the assessment of coronary arteries, while the UHR mode reduced blooming artifacts and improved the evaluation of coronary stents compared to conventional EID-CT [6–8]. However, the optimal kernel, QIR and slice thickness setting is not yet defined for clinical use for either native coronaries or stented segments. Also, there are limited data on the impact of using different protocols on quantitative image quality parameters.

Our aim was to identify the optimal reconstruction settings, based on qualitative and quantitative image quality parameters, for the assessment of coronary arteries and stents acquired by PCCT. We examined the effects of different kernels, slice thicknesses, and iterative reconstruction settings on both standard and UHR images.

2. Material and methods

2.1. Study population

Between November 2022 and January 2023, we retrospectively enrolled 45 patients with suspected or known CAD and stable symptoms who were referred for clinically indicated coronary CTA. These patients were selected from a single-center study, following exclusion criteria (images with severe motion artefacts were excluded n = 12 and an additional 5 patients underwent focused scans for prosthetic valve evaluation). Two groups were included: 1) Patients with standard coronary CTA protocol for quantitative and qualitative image quality evaluation and 2) patients with coronary stents undergoing UHR protocol for coronary stent evaluation, including blooming assessment and quantitative and qualitative image quality of the coronaries. The study was approved by the institutional ethical committee (IV/667–1/2022/EKU) and was performed in accordance with the Helsinki declaration. Written informed consent was waived from all patients due to the retrospective nature of our study.

2.2. Coronary CTA acquisition protocols

Coronary CTA imaging of the heart was performed using dual-source PCCT system (NAEOTOM Alpha, Siemens Healthineers) according to the guidelines of the Society of Cardiovascular Computed Tomography [9]. Prior to the examination all patients received 0.8 mg sublingual nitroglycerine and received oral or intravenous metoprolol if the heart rate (HR) was more than 65 beats/minute, in the absence of contraindications. The acquisition protocol included an unenhanced CT scan

Table 1
Reconstruction parameters and kernels for standard and UHR acquisition mode.

Scan mode	Standard - reconstructed at 70 keV				Ultra-high resolution			
Image matrix	512 x 512				512 x 512			
Slice thickness	0.4 mm		0.6 mm		0.2 mm		0.4 mm	
Convolution kernel	Bv40	Bv44	Bv40	Bv44	Bv44	Bv56	Bv44	Bv56
Iterative reconstruction	QIR 0–4	QIR 0–4	QIR 0–4	QIR 0–4	QIR 0–4	QIR 0–4	QIR 0–4	QIR 0–4

Table 2
Patient characteristics and CT scan parameters.

Demographic data	Patient population n = 45
Age, years	62.8 ± 10.8
Male sex	30 (67 %)
BMI, kg/m^2	27.7 ± 3.3
Hypertension	36 (80 %)
Diabetes mellitus	9 (20 %)
Dyslipidemia	19 (42 %)
Smoking	5 (11 %)
CT scan parameters	
DLP, mGy*cm^2	262 ± 194
Effective dose, mSv	3.7 ± 2.7
Mean HR during scan, beats/min	62 ± 7

BMI: Body mass index; DLP: Dose length product; HR: Heart rate.

followed by 1) a standard coronary CTA acquisition mode or 2) an UHR acquisition mode in the presence of coronary stent.

Standard CTA acquisition parameters were the following: tube voltage = 140 kVp, automatic tube current modulation with image quality level (IQ-level) = 64, detector configuration = 144 × 0.4 mm, rotation time = 0.25 s. Based on patients' HR, different scan modes were applied: high-pitch helical (TurboFlash) scan mode in case of regular HR < 70/min, sequential scan mode in case of HR > 70/min. Images with sequential acquisition protocol were acquired in diastole (65–85 % of the R-R interval) or systole (200——400 ms) depending on the HR (<or > 75 beats/minute).

UHR acquisition settings were as follows: tube voltage = 140 kVp, automatic tube current modulation with IQ-level = 64, detector configuration = 120 x 0.2 mm, rotation time = 0.25 s using sequential or helical scan mode depending on patients' HR (Sequential scan mode for ≤ 70/min and spiral acquisition for HR > 70/min).

A four-phasic contrast injection protocol was used with 70–80 ml contrast agent at a flow rate of 4.5–5.0 ml/s [10].

2.3. Coronary CTA reconstruction

In each case, cardiac cycle phases with the least motion artifacts were reconstructed and included in the analysis. We selected a smoother and a sharper kernel setting based on our routine clinical protocol.1) Standard images were reconstructed using slice thickness of 0.4 mm (0.4 mm increment) or 0.6 mm (0.4 mm increment), with two different vascular kernels (Bv40 or Bv44) and a novel QIR algorithm with strength levels from 0 to 4. All images were reconstructed at 70 keV using a matrix of 512 x 512 with identical field-of-view (FOV of 200 mm). The influence of various virtual monoenergetic reconstructions on image quality has been previously published (19).

2) UHR images were reconstructed using slice thickness of 0.2 mm (0.2 mm increment) or 0.4 mm (0.4 mm increment), with two different vascular kernels (Bv44 or Bv56) and QIR algorithm with strength levels from 0 to 4 (Fig. 1). All images were reconstructed using a matrix of 512 x 512 and identical FOV.

The predefined image reconstruction settings are summarized in Table 1.

2.4. Qualitative image quality analysis

Qualitative image quality analysis of all images was performed by two experienced readers in cardiovascular CT imaging (B.S. 9 years' experience in cardiovascular imaging and B.V. 6 years' experience in cardiovascular imaging) blinded to reconstruction data. Images were independently scored by the two readers according to a 4-point Likert scale (1-poor; 2-average; 3-good; 4-excellent) for the evaluation of coronary arteries on the standard resolution images (overall image appearance describing graininess, sharpness, and lumen definition), and for the assessment of coronary stents on the UHR. We then summed the scores from both readers to determine the highest overall image quality based on subjective evaluation. ***Quantitative image quality assessment.***

Quantitative image quality analysis was performed for all reconstructed images using the Syngo.via workstation (version VB60A, Siemens Healthineers) by a single reader with 5 years' experience in cardiovascular CT imaging. Image noise, signal-to-noise ratio (SNR) and contrast-to-noise ratio (CNR) were assessed for proximal and distal segments of the 3 main coronary vessels (left anterior descending [LAD], left circumflex [LCX] and right coronary artery [RCA]). Circular region of interest (ROI; 200 mm^2) was placed in the aortic root at the level of the left main coronary ostium for the assessment of image noise defined as the standard deviation (SD_{aorta}) of attenuation values. Mean attenuation in Hounsfield unit (HU) was measured by placing circular ROIs in the coronary lumen (HU_{lumen}) and pericoronary fat (HU_{fat}) in proximal and distal segments of LAD (pLAD, dLAD), LCX (pLCX, dLCX) and RCA (pRCA, dRCA). Artifacts and plaques were carefully avoided while manually placing ROIs into the coronary lumen. ROIs were copied and pasted to the same position on all reconstructed images for identical measurement of SD_{aorta} and HU values. SNR and CNR were calculated for all reconstructed images as following: $SNR = HU_{lumen}/SD_{aorta,}$ and $CNR = (HU_{lumen} - HU_{fat}) / SD_{aorta}$.

2.5. Stent assessment using ultra-high resolution

On UHR datasets, image quality of coronary stents was evaluated as well. Circular ROIs were placed in the stent lumen and in the coronary lumen proximal to the stent for image noise (SD) and mean attenuation (HU) measurements (SD_{stent}, $SD_{peristent}$, HU_{stent}, $HU_{peristent}$). CNR was calculated for each stent as $CNR = (HU_{stent} - HU_{fat}) / SD_{stent}$. The effect of stent-induced artifact on lumen image quality was assessed by calculating the difference between intrastent attenuation and peristent attenuation: $\Delta HU_{stent} = HU_{stent} - HU_{peristent}$ [11,12].

2.6. Statistical analysis

Continuous variables are presented as mean and standard deviation, whereas categorical parameters are presented as frequency with percentages. We used repeated measures Analysis of Variances (ANOVA) and post-hoc comparison analysis (Bonferroni) to compare quantitative image quality parameters between the different reconstructions. Relative percentage change was calculated between different QIR levels, slice thickness and kernel settings. The average HU, CNR and SNR of the proximal (pLAD, pLCX, pRCA) versus distal (dLAD, dLCX, dRCA) coronary segments were compared using paired *t*-test. The intra-reader reproducibility between image quality measurements (median vascular attenuation and CNR) was calculated on 20 datasets (10

Fig. 2. Plot shows the results of subjective image quality assessment of standard (coronary lumen) and UHR (stents) images. Each bar indicates the frequency of a score assigned by a reader for a reconstruction. Colors represent image quality as follows: green – excellent; yellow – good; orange – average; red – poor quality. (For interpretation of the references to colour in this figure legend, the reader is referred to the web version of this article.)

Standard and 10 UHR images were randomly selected) using intraclass correlation coefficient (ICC). The following descriptive scale was used for values of the correlation coefficient: < 0.90 poor, 0.90–0.94 moderate, 0.95–0.99 excellent, >0.99 almost perfect. Inter-reader agreement between two readers was assessed on 20 cases using Cohen's kappa. All statistical analyses were performed using IBM SPSS Statistics (version 25). A two-sided $p < 0.05$ was considered as statistically significant.

3. Results

A total of 45 patients were evaluated after excluding 12 images with severe motion artefacts and an additional 5 patients who underwent focused scans for prosthetic valve evaluation: 29 patients were scanned using standard and 16 with UHR scan mode (67 % male, mean age of 62.8 ± 10.8 years, mean DLP: 262 ± 194 mGy*cm^2). The image quality analysis included 270 coronary segments (45 patients x 6 segments) and 23 stents from the 16 included patients. Patient characteristics and scan

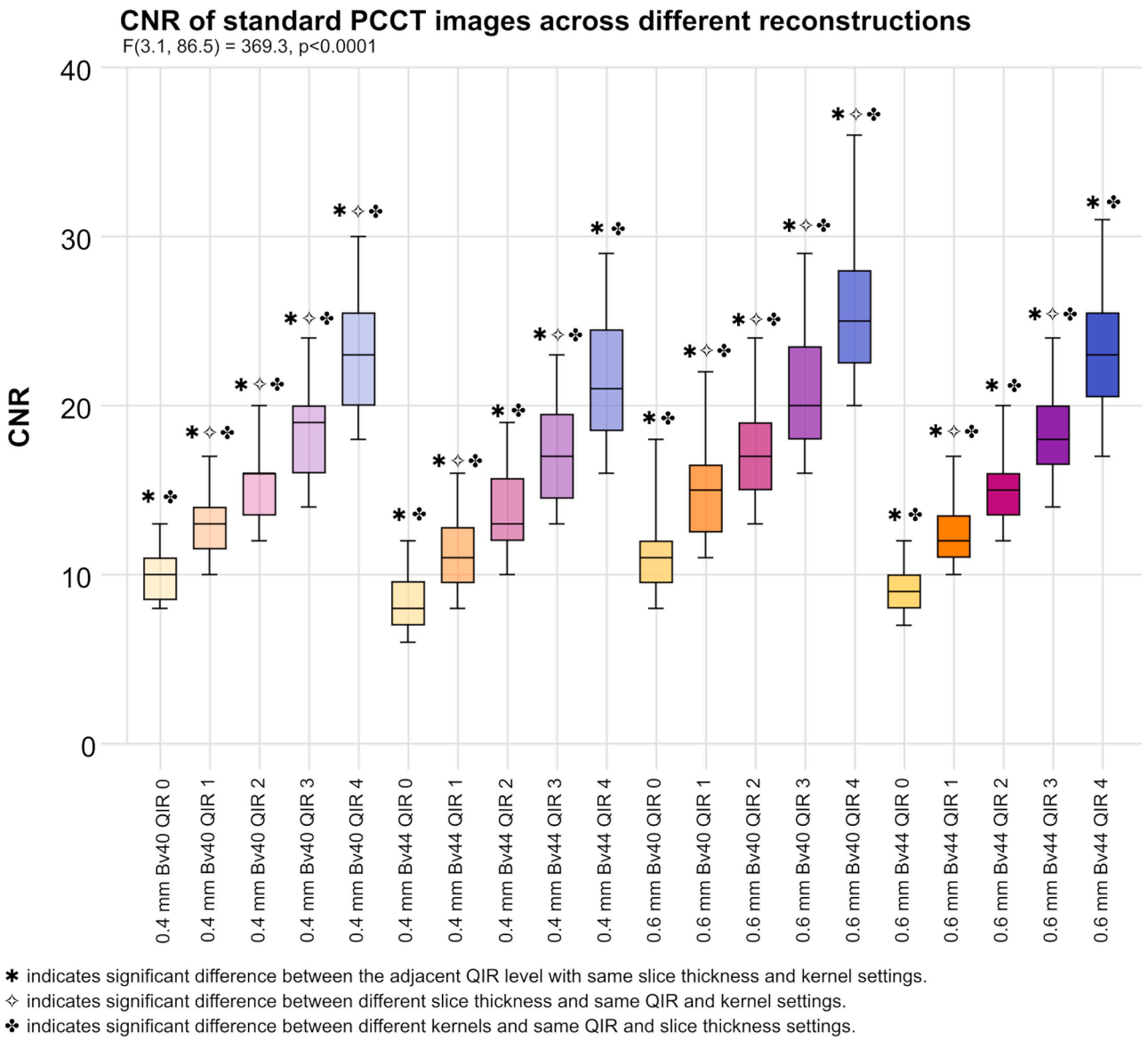

Fig. 3. Box plot demonstrating differences in CNR of coronaries using different kernels, QIR level and slice thickness on standard PCCT images.

parameters are described in Table 2.

3.1. Qualitative image quality

The highest overall image quality, as subjectively assessed for coronary arteries, was found in images reconstructed with Bv44 kernel and QIR 3 or QIR 4 with both 0.4 mm and 0.6 mm slice thicknesses (97 % excellent) for the standard resolution. The mean Likert score values were the highest for 0.6 mm, Bv44 and QIR 3/4 (3.97 ± 0.18) and 0.4 mm, Bv44 and QIR 3/4 (3.97 ± 0.17), and the lowest for 0.6 mm, Bv40 and QIR off (2.53 ± 0.57).

For the UHR mode, the highest quality was achieved with 0.2 mm, Bv56 and QIR 4 (3.91 ± 0.28, 92 % excellent), whereas the lowest score was detected using 0.2 mm Bv44 QIR off (1.50 ± 0.49). When only analysing the QIR level 4 images, readers preferred Bv56 over Bv44 for coronary CTA reads (Fig. 2).

3.2. Image quality evaluation using standard reconstruction

In the standard acquisition group mean image noise decreased, while SNR and CNR increased significantly with increasing QIR levels (CNR values are shown on Fig. 3). Larger slice thickness resulted in substantially decreased image noise and increased SNR and CNR values, while sharper kernel (Bv44 vs Bv40) significantly increased image noise and decreased CNR and SNR for all 3 coronary vessels (Table 3).

The highest mean CNR was measured on 0.6 mm slice thickness images with Bv40 kernel and QIR 4 reconstruction and lowest on 0.4 mm Bv44 and QIR 0 settings: 25.8 ± 4.1 vs. 8.3 ± 1.6, respectively ($p < 0.001$). There was a significant increase in CNR by an average of 11.7 % when changing from 0.4 mm to 0.6 mm slice thickness within the same QIR and kernel settings (mean difference: 1.9; confidence interval (CI): 0.6—–3.3; $p < 0.05$), except in case of Bv40 / QIR 0 and Bv44 / QIR 0, QIR 2 and QIR 4 ($p > 0.05$). Transitioning from a medium smooth kernel (Bv40) to sharper kernel (Bv44) resulted in a significant decrease in CNR by an average 8.7 % (mean difference: −1.6; CI: −2.9 - −0.4; $p < 0.01$). One step increase in QIR level reached an average 25.2 % increase in CNR with significant difference between each step for both smooth and sharper kernel settings and both slice thickness ($p < 0.0001$ for all).CNR improved by an average 144.7 % from QIR level 0 to 4 (mean difference: 13.7; CI: 11.1—–16.4; $p < 0.001$). Images with slice thickness of 0.4 mm maintained high CNR using QIR level 3–4: for QIR 3 18.5 ± 2.8 on Bv40 and 16.9 ± 3.0 on Bv44 images; for QIR 4: 23.1 ± 3.6 for Bv40 and 21.5

Table 3
Quantitative image quality parameters of standard coronary CTA images.

Parameters	Standard reconstruction 0.4 mm Bv 40					Standard reconstruction 0.6 mm Bv 40				
	QIR 0	QIR 1	QIR 2	QIR 3	QIR 4	QIR 0	QIR 1	QIR 2	QIR 3	QIR 4
Aorta SD	56.7 ± 8.8	44.0 ± 7.0	37.8 ± 5.9	31.7 ± 5.1	25.7 ± 4.4	49.6 ± 8.1	38.6 ± 6.2	33.4 ± 5.0	28.1 ± 4.4	23.0 ± 3.7
Mean HU										
LAD	432.4 ± 84.7	449.9 ± 89.6	453.2 ± 90.6	457.1 ± 91.4	461.4 ± 92.7	428.4 ± 78.7	445.7 ± 83.2	449.4 ± 85.3	453.9 ± 86.7	459.9 ± 87.8
LCX	438.5 ± 72.5	456.0 ± 76.6	458.3 ± 77.1	462.2 ± 78.3	466.2 ± 79.5	432.9 ± 72.6	452.0 ± 77.1	455.0 ± 78.3	459.4 ± 79.5	463.8 ± 80.8
RCA	467.2 ± 91.7	488.7 ± 94.8	492.8 ± 94.9	498.7 ± 95.5	504.5 ± 96.1	462.1 ± 90.6	484.1 ± 93.5	488.4 ± 93.7	494.3 ± 94.2	500.2 ± 94.8
Mean CNR										
LAD	9.6 ± 1.7	12.9 ± 2.2	15.1 ± 2.6	18.1 ± 3.2	22.6 ± 4.1	11.1 ± 2.4	14.7 ± 3.0	17.0 ± 3.1	20.4 ± 3.8	25.2 ± 4.6
LCX	9.7 ± 1.7	12.9 ± 2.1	15.1 ± 2.5	18.1 ± 3.0	22.6 ± 3.8	10.9 ± 2.2	14.6 ± 2.7	16.9 ± 2.8	20.3 ± 3.4	25.0 ± 4.2
RCA	10.2 ± 1.6	13.7 ± 2.2	16.1 ± 2.5	19.4 ± 3.0	24.3 ± 3.9	11.7 ± 2.5	15.7 ± 3.1	18.2 ± 3.2	21.9 ± 3.8	27.0 ± 4.6
Mean SNR										
LAD	7.9 ± 1.6	10.5 ± 2.1	12.4 ± 2.4	14.9 ± 2.9	18.5 ± 3.7	9.0 ± 2.2	12.0 ± 2.8	14.0 ± 2.9	16.7 ± 3.5	20.7 ± 4.1
LCX	8.0 ± 1.4	10.7 ± 2.0	12.6 ± 2.2	15.0 ± 2.5	18.7 ± 3.2	9.0 ± 2.1	12.2 ± 2.6	14.2 ± 2.6	17.0 ± 3.1	20.9 ± 3.8
RCA	8.5 ± 1.5	11.4 ± 2.0	13.4 ± 2.4	16.2 ± 2.8	20.2 ± 3.6	9.7 ± 2.3	13.0 ± 2.9	15.1 ± 3.0	18.2 ± 3.5	22.4 ± 4.3
Parameters	Standard reconstruction 0.4 mm Bv 44					Standard reconstruction 0.6 mm Bv 44				
	QIR 0	QIR 1	QIR 2	QIR 3	QIR 4	QIR 0	QIR 1	QIR 2	QIR 3	QIR 4
Aorta SD	70.0 ± 12.7	53.6 ± 9.7	45.3 ± 8.1	37.4 ± 6.6	30.0 ± 5.4	63.3 ± 9.9	48.1 ± 7.4	41.0 ± 6.3	34.1 ± 5.3	27.6 ± 4.4
Mean HU										
LAD	449.1 ± 91.1	473.8 ± 98.2	487.5 ± 101.9	495.3 ± 103.7	503.1 ± 105.7	444.4 ± 83.9	470.3 ± 91.5	484.5 ± 95.1	492.3 ± 97.1	500.4 ± 99.6
LCX	457.6 ± 77.7	484.2 ± 84.1	498.4 ± 87.3	506.3 ± 88.9	513.6 ± 90.6	451.9 ± 77.0	479.1 ± 83.8	494.0 ± 87.0	501.5 ± 88.6	509.6 ± 91.0
RCA	478.6 ± 95.5	504.3 ± 100.4	518.3 ± 103.0	526.5 ± 104.0	534.9 ± 105.0	473.5 ± 94.7	500.5 ± 99.1	515.1 ± 101.4	523.5 ± 102.2	532.2 ± 103.2
Mean CNR										
LAD	8.1 ± 1.6	11.1 ± 2.2	13.5 ± 2.6	16.6 ± 3.1	21.0 ± 3.9	8.9 ± 1.5	12.2 ± 2.1	14.8 ± 2.5	18.0 ± 3.0	22.6 ± 3.9
LCX	8.2 ± 1.8	11.3 ± 2.4	13.7 ± 2.7	16.8 ± 3.2	21.2 ± 3.9	8.8 ± 1.5	12.3 ± 2.1	14.8 ± 2.5	18.1 ± 2.9	22.7 ± 3.7
RCA	8.5 ± 1.7	11.7 ± 2.3	14.2 ± 2.7	17.4 ± 3.2	22.0 ± 3.9	9.3 ± 1.6	12.8 ± 2.2	15.5 ± 2.6	18.9 ± 3.0	23.8 ± 3.8
Mean SNR										
LAD	6.7 ± 1.5	9.2 ± 2.0	11.2 ± 2.4	13.7 ± 2.9	17.3 ± 3.6	7.2 ± 1.4	10.1 ± 1.9	12.2 ± 2.3	14.8 ± 2.8	18.7 ± 3.6
LCX	6.8 ± 1.5	9.5 ± 2.0	11.4 ± 2.3	14.1 ± 2.9	17.8 ± 3.4	7.4 ± 1.5	10.4 ± 1.9	12.5 ± 2.2	15.1 ± 2.6	19.1 ± 3.5
RCA	7.1 ± 1.5	9.8 ± 2.0	11.9 ± 2.4	14.6 ± 2.8	18.4 ± 3.4	7.7 ± 1.4	10.7 ± 2.0	12.9 ± 2.4	15.8 ± 2.8	19.8 ± 3.4

CNR: Contrast-to-noise ratio; CTA: CT angiography; HU: Hounsfield unit; LAD: Left anterior descending; LCX: Left circumflex; QIR: Quantum iterative reconstruction; RCA: Right coronary artery; SD: Standard deviation; SNR: Signal-to-noise ratio.

± 3.7 for Bv44 images.

When comparing proximal and distal coronary segments, no significant difference was observed in mean HU for the RCA when using a sharper convolution kernel (Bv44) and QIR levels 1–4 with 0.4 mm slice thickness, and QIR levels 2–4 with 0.6 mm slice thickness images.Image quality, as assessed by CNR and SNR, remained excellent when comparingproximal and distal segments of the RCA on images with sharper Bv44 kernel and QIR level 3–4 ($p > 0.05$). On the other hand, CNR values were lower for distal segments of LAD and LCX as compared to the proximal segments ($p < 0.05$) (Supplementary table 1 and 2).

3.3. Image quality evaluation using UHR

Overall image quality of UHR images showed similar tendency to standard images. with higher QIR levels resulting in substantially higher SNR and CNR values (CNR values are shown on Fig. 4). Similarly, higher slice thickness resulted in significantly decreased image noise and increased SNR and CNR values, while sharper kernel (Bv56 vs Bv44) significantly increased image noise and decreased CNR and SNR for all 3 coronary vessels (Table 4).

The highest mean CNR was observed on 0.4 mm slice thickness with Bv40 kernel and QIR 4 and lowest on 0.2 mm, Bv56 and QIR 0 images: 21.5 ± 3.9 vs. 3.6 ± 0.8, respectively ($p < 0.001$). Increasing the slice thickness from 0.2 mm to 0.4 mm resulted in a significant mean increase in CNR of 29.5 % (mean difference: 4.2; CI: 1.2—–7.2; $p < 0.001$). Using a sharper kernel (from Bv44 to Bv56) significantly decreased CNR with a mean of 41.2 % (mean difference: −5.8; CI: −8.8 - −2.9; $p < 0.001$).

Each step increase in QIR level was associated with an average 26.7 % increase in CNR with significant differences observed between each step for both kernel settings and both slice thicknesses ($p < 0.0001$ for all). A significant difference was observed between QIR level 0 to 4 by an average 158.0 % for all evaluated segments (mean difference: 9.5; CI: 6.5—–12.4; $p < 0.001$). Using QIR level 4, images preserved high CNR also on 0.2 mm slice thickness images: 17.9 ± 3.0 for Bv44 kernel.

Proximal versus distal RCA segments showed no significant difference in CNR and SNR through all reconstructed images ($p > 0.05$). Comparing proximal and distal segments of LAD and LCX, using sharper kernels (Bv56) and higher QIR level (level 4) settings also showed tendency in maintaining image quality for distal coronary segments (Supplementary table 3 and 4).

3.4. Image quality analysis of coronary stents

Similar trends were observed when evaluating coronary stents on UHR images. The comparison of CNR values across different reconstructions is demonstrated on Fig. 5. The highest CNR of coronary stents was observed on 0.4 mm slice thickness, Bv44 and QIR 4 images, while lowest was measured on 0.2 mm slice thickness, Bv56 and QIR 0 images: 18.9 ± 6.3 vs. 4.3 ± 1.5 ($p < 0.001$).

The difference between the attenuation measured in the stent lumen and coronary lumen adjacent to the stent (ΔHU_{stent}) decreased with increasing QIR levels, with sharper kernel (Bv56) and with larger slice thickness. The lowest ΔHU_{stent} was measured using 0.4 mm slice thickness, Bv56 and QIR level 2–4 (mean ΔHU_{stent}: 7.4 ± 41.4; −0.6 ±

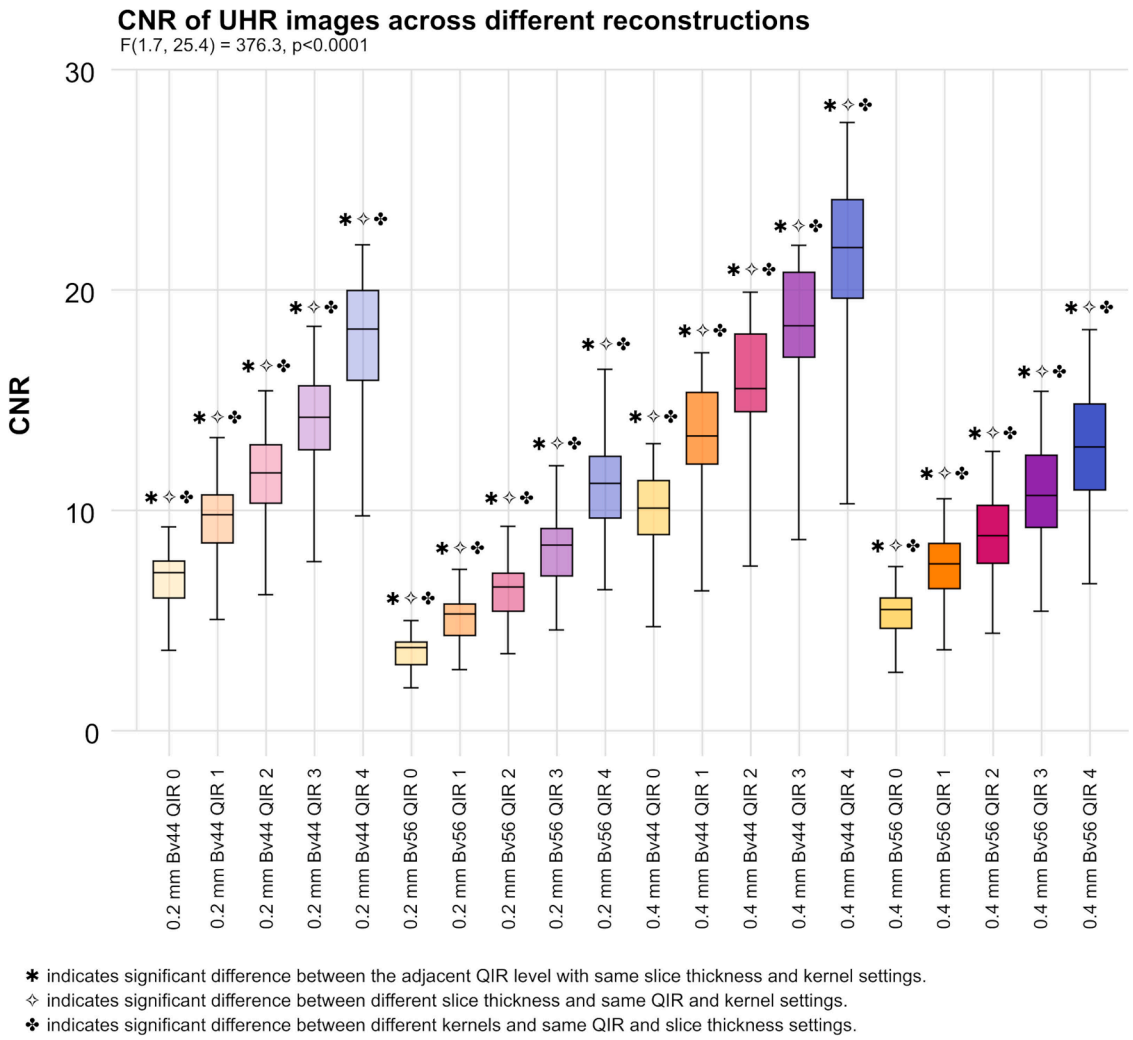

Fig. 4. Box plot demonstrating differences in CNR of coronaries using different kernels, QIR level and slice thickness on UHR PCCT images.

42.6; −8.7 ± 45.3, respectively) and using 0.2 mm slice thickness with Bv56 and QIR level 4 (mean ΔHU_{stent}: 5.7 ± 38.6). While highest ΔHU_{stent} was found on 0.4 mm slice thickness, Bv44 and QIR level 0 images: −8.7 ± 45.3 vs. 62.0 ± 54.1 (all comparisons $p < 0.01$) (Table 4).

3.5. Reproducibility of image quality parameters

Intra-observer agreement for mean attenuation, SNR and CNR was excellent (ICC: 0.97–0.98). Kappa value was 0.71 for standard and 0.79 for UHR reconstructions.

4. Discussion

PCCT is increasingly being incorporated into clinical practice and has the potential to overcome current limitations of coronary CTA [13]. However, data on optimizing post-processing reconstruction settings for analysing coronary arteries and stents are acarce. In our study we provided a comprehensive image quality evaluation of coronaries using the first generation dual-source PCCT. We evaluated the impact of different kernel, iterative reconstruction and slice thickness settings on qualitative and quantitative image quality parameters of coronary arteries with and without stents for both standard and UHR images. Additionally, we aimed to evaluate differences in CNR between proximal and distal segments. Two experienced readers independently assessed the images for overall image quality to establish a subjective set of optimal reconstructions.

Photon-counting detector CT technology can minimize electronic noise and allows for higher spatial resolution resulting in better vessel visualization, improved noise characteristics and decreased blooming due to higher spatial resolution [4]. Conventional EID-CT technology has a limit of 0.6 mm for high resolution imaging without the application of comb filters, however current PCCT scanner technology provides a slice thickness of 0.4 mm using standard acquisition mode and 0.2 mm with UHR mode owing to the novel detector design with smaller pixels. A novel iterative reconstruction technique (quantum iterative reconstruction) was developed to compensate for increasing image noise when reconstructing thinner slices. Large variety of kernel and QIR settings exists across sites therefore better understanding of the optimal combination is essential to ensure best practice using this novel technique and for further studies on coronaries using PCCT.

Increasing the levels of QIR provides significant improvement in image quality based on on both standard and UHR images. We found that applying QIR level 4 led to a greater than twofold increase in CNR as compared to FBP (QIR off) on 0.4 mm slice thickness. Although utilizing thinner slice thickness and sharper kernels for the evaluation of coronary arteries decrease SNR and CNR values, both standard and UHR images maintained high image quality using higher QIR levels, combining the advantage of higher spatial resolution and decreased noise.

Despite increased CNR values were seen for the larger slice thickness images or smoother kernels, the subjective evaluation revealed that

Table 4
Quantitative image quality parameters of UHR coronary CTA images.

Parameters	**Ultra-high resolution 0.2 mm Bv 44**					**Ultra-high resolution 0.4 mm Bv 44**				
	QIR 0	QIR 1	QIR 2	QIR 3	QIR 4	QIR 0	QIR 1	QIR 2	QIR 3	QIR 4
Aorta SD	65.3 ± 13.0	49.8 ± 9.7	42.1 ± 8.1	34.9 ± 6.5	27.9 ± 5.1	45.2 ± 10.8	35.8 ± 8.3	31.4 ± 7.1	27.4 ± 6.2	23.7 ± 5.4
Mean HU										
LAD	368.3 ± 94.3	384.4 ± 91.1	393.1 ± 89.8	397.6 ± 89.6	401.3 ± 89.6	369.2 ± 90.4	388.1 ± 87.6	397.8 ± 86.7	402.2 ± 86.7	406.3 ± 86.7
LCX	363.0 ± 86.9	381.0 ± 91.3	392.8 ± 91.9	397.4 ± 93.1	402.1 ± 94.5	355.1 ± 83.8	377.3 ± 89.6	388.6 ± 92.5	393.4 ± 94.5	398.4 ± 96.6
RCA	386.6 ± 74.3	401.6 ± 75.8	407.9 ± 79.1	413.9 ± 78.1	418.2 ± 78.7	380.2 ± 70.4	400.2 ± 74.2	410.3 ± 76.8	415.6 ± 77.9	421.0 ± 79.2
Mean CNR										
LAD	6.8 ± 1.6	9.4 ± 2.1	11.4 ± 2.4	14.0 ± 2.8	17.6 ± 3.3	10.0 ± 2.1	13.4 ± 2.7	15.7 ± 3.1	18.2 ± 3.4	21.4 ± 3.9
LCX	6.7 ± 1.4	9.3 ± 1.9	11.4 ± 2.4	13.9 ± 2.8	17.6 ± 3.4	9.6 ± 2.1	13.0 ± 2.8	15.3 ± 3.3	17.9 ± 3.8	21.0 ± 4.5
RCA	7.1 ± 1.4	10.3 ± 3.1	11.9 ± 2.2	14.5 ± 2.6	18.3 ± 3.1	10.3 ± 2.0	13.7 ± 2.5	16.1 ± 3.0	18.7 ± 3.3	22.0 ± 3.9
Stent	9.9 ± 5.2	13.2 ± 9.6	13.5 ± 6.3	14.5 ± 5.6	15.5 ± 5.9	13.1 ± 4.2	16.3 ± 5.3	17.4 ± 6.0	18.1 ± 7.4	18.9 ± 6.3
Mean SNR										
LAD	5.8 ± 1.8	8.0 ± 2.2	9.6 ± 2.6	11.7 ± 3.0	14.7 ± 3.6	8.5 ± 2.5	11.3 ± 3.0	13.1 ± 3.3	15.2 ± 3.7	17.7 ± 4.1
LCX	5.7 ± 1.7	7.9 ± 2.3	9.7 ± 2.7	11.7 ± 3.2	14.8 ± 3.9	8.2 ± 2.5	11.0 ± 3.2	12.9 ± 3.6	15.0 ± 4.1	17.5 ± 4.8
RCA	6.1 ± 1.4	8.3 ± 1.9	9.9 ± 2.3	12.1 ± 2.7	15.2 ± 3.2	8.7 ± 2.1	11.5 ± 2.6	13.4 ± 3.0	15.6 ± 3.4	18.2 ± 3.9
Mean ΔHU_{stent}	58.3 ± 53.4	38.3 ± 42.6	27.8 ± 41.1	25.3 ± 42.4	22.5 ± 44.9	62.0 ± 54.1	33.9 ± 50.9	20.1 ± 52.9	15.4 ± 56.3	10.8 ± 60.6

Parameters	**Ultra-high resolution 0.2 mm Bv 56**					**Ultra-high resolution 0.4 mm Bv 56**				
	QIR 0	QIR 1	QIR 2	QIR 3	QIR 4	QIR 0	QIR 1	QIR 2	QIR 3	QIR 4
Aorta SD	133.2 ± 27.0	96.1 ± 19.3	78.5 ± 15.4	60.9 ± 11.8	45.1 ± 8.3	89.1 ± 20.1	67.1 ± 15.4	57.8 ± 13.0	48.4 ± 10.6	41.1 ± 8.7
Mean HU										
LAD	394.5 ± 87.0	407.0 ± 82.8	414.2 ± 81.1	418.3 ± 80.2	422.2 ± 79.8	392.7 ± 80.9	411.0 ± 78.6	420.8 ± 78.2	426.8 ± 78.1	431.6 ± 78.3 s
LCX	384.6 ± 92.2	397.5 ± 93.8	404.7 ± 95.0	409.2 ± 95.7	413.1 ± 96.5	378.4 ± 85.8	397.3 ± 91.7	407.6 ± 95.0	413.2 ± 97.4	418.7 ± 99.9
RCA	395.7 ± 75.5	404.4 ± 73.8	409.8 ± 73.6	411.5 ± 72.2	416.3 ± 73.0	390.3 ± 71.4	405.5 ± 73.3	414.0 ± 74.9	419.0 ± 75.7	424.1 ± 76.8
Mean CNR										
LAD	3.6 ± 0.9	5.2 ± 1.3	6.4 ± 1.6	8.4 ± 2.0	11.4 ± 2.6	5.4 ± 1.3	9.0 ± 2.1	11.0 ± 2.5	10.9 ± 2.5	13.1 ± 3.0
LCX	3.5 ± 0.8	5.1 ± 1.2	6.3 ± 1.5	8.2 ± 1.9	11.1 ± 2.5	5.2 ± 1.2	7.3 ± 1.8	8.7 ± 2.1	10.6 ± 2.6	12.7 ± 3.0
RCA	3.6 ± 0.8	5.2 ± 1.1	6.4 ± 1.4	8.3 ± 1.8	11.3 ± 2.4	5.4 ± 1.2	7.5 ± 1.6	8.9 ± 1.9	10.8 ± 2.3	12.9 ± 2.7
Stent	4.3 ± 1.5	5.7 ± 2.0	6.8 ± 2.6	8.1 ± 3.1	10.1 ± 4.0	6.3 ± 1.8	8.0 ± 2.3	9.0 ± 2.8	10.4 ± 3.5	12.0 ± 4.1
Mean SNR										
LAD	3.1 ± 0.9	4.4 ± 1.2	5.5 ± 1.5	7.1 ± 1.9	9.6 ± 2.5	4.6 ± 1.3	6.4 ± 1.8	7.6 ± 2.0	9.1 ± 2.4	10.9 ± 2.8
LCX	3.0 ± 0.9	4.3 ± 1.3	5.4 ± 1.6	7.0 ± 2.0	9.5 ± 2.7	4.5 ± 1.3	6.2 ± 1.9	7.4 ± 2.2	8.9 ± 2.6	10.6 ± 3.1
RCA	3.1 ± 0.8	4.4 ± 1.1	5.4 ± 1.3	7.0 ± 1.7	9.5 ± 2.3	4.5 ± 1.2	6.3 ± 1.6	7.4 ± 1.9	9.0 ± 2.2	10.7 ± 2.6
Mean ΔHU_{stent}	46.4 ± 61.5	28.2 ± 47.1	17.7 ± 42.0	11.7 ± 39.1	5.7 ± 38.6	48.2 ± 51.9	21.6 ± 42.8	7.4 ± 41.4	−0.6 ± 42.6	−8.7 ± 45.3

CNR: Contrast-to-noise ratio; CTA: CT angiography; HU: Hounsfield unit; LAD: Left anterior descending; LCX: Left circumflex; UHR: Ultra-high resolution; QIR: Quantum iterative reconstruction; RCA: Right coronary artery; SD: Standard deviation; SNR: Signal-to-noise ratio.

readers prefer 0.4 mm Bv44 QIR 3/4 or 0.6 mm Bv44 QIR 3/4 for the standard, and 0.2 mm Bv56 QIR 4 for UHR images. This can be explained due to the better lumen delineation on sharper images for clinical reads. Previous investigations found similar image quality with high CNR using 0.4 mm slice thickness, medium smooth kernel (Bv40) and QIR level 3 [14]. Mergen et al performed image quality assessment focusing on the kernel selection of UHR using a different set of kernels (Bv40, Bv44, Bv56, Bv60, Bv64, Bv72, Bv80, and Bv89) and a QIR level of 4 [6]. The maximum spatial frequency (f_{peak}) increased using sharper kernels Bv40 to Bv64, but not for reconstructions with the Bv72 to Bv89 (1024x1024 matrix) kernels using a tube voltage of 120 kVp. Blooming artifacts decrease, while sharpness increases with higher kernel numbers as expected. Bv64 (a FOV of 200 x 200 mm^2, matrix size of 512 x 512 pixels) was selected as an optimal kernel for the morphological analysis of plaque with a QIR level of 4. Bv56 renders comparable lp/cm values and blooming as Bv64, while CNR drops from 12.5 ± 2.6 to 8.1 ± 1.8 using Bv64 instead of Bv56. Also, the use of Bv64 or sharper kernels could be limited in case of overweight patients (BMI above 25 kg/m^2). The same study group analyzed in-stent lumen visualization and identified Bv72 kernel at 0.2 mm as an optimal reconstruction based on subjective assessment and in-stent lumen diameter measurements [15]. These results suggest that native coronary lumen and the adjacent plaque evaluation should be performed on a different kernel setting as in-stent lumen evaluation using PCCT. Notably, current UHR does not allow for spectral image analysis using different virtual monoenergetic images or other post processing tools such as PureCalcium or PureLumen as with standard collimation mode [16]. We selected a smoother and sharper kernel with different slice thickness pre-specified for the UHR or standard scan mode and our readers preferred sharper kernels and thinner slice thickness despite lower CNR for the analysis of coronary lumen based on subjective evaluation.

Our investigation also compared quantitative image quality of proximal and distal coronary segments. Based on our results, CNR values in the proximal versus distal segments did not differ significantly when applying sharper kernels and thinner slice thickness combined with QIR in case of the RCA (see Supplemental material). When analysing the LCX and the LAD, CNR values differed for most reconstructions. However, with a 0.4 mm slice thickness using the UHR mode and a high level of QIR (4) we could not detect significant difference between the proximal and distal vessel segments in CNR. The difference between the left and right coronary system could be due to the commonly greater vessel caliber of distal RCA compared to either distal LAD or LCX. These findings suggest excellent distal vessel visualization for the clinical evaluation of coronaries. Soschynski et al. performed subjective image

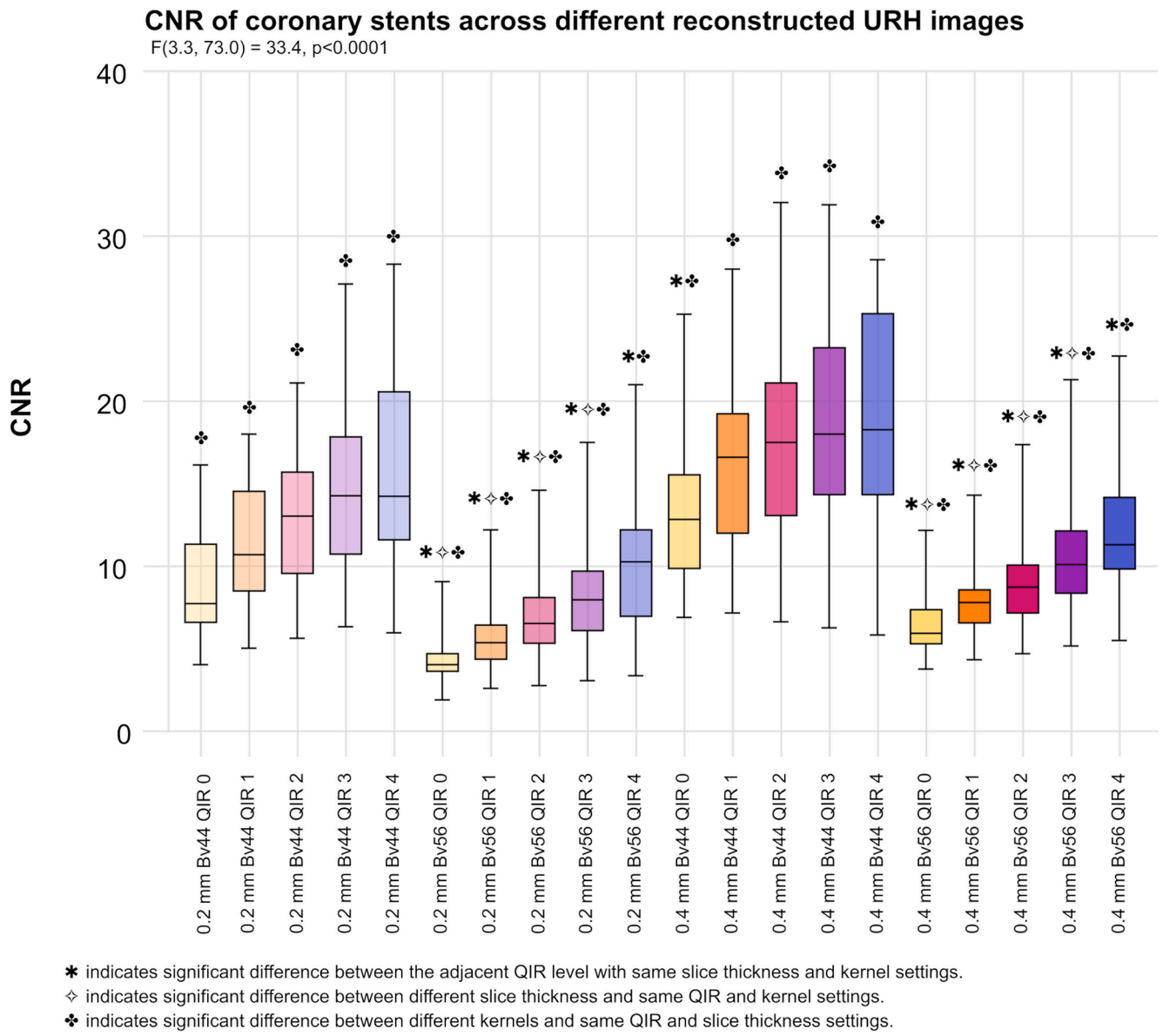

Fig. 5. Box plot demonstrating differences in CNR of coronary stents using different kernels, QIR level and slice thickness on UHR PCCT images.

quality assessment of 92 coronary CTA images using PCCT and found that the distal coronary segments exhibited significantly lower image quality than the proximal segments [14]. Notably, in their study they only evaluated one reconstruction setting using monoenergetic images at 60 keV, 0.4 mm slice thickness, Bv40 kernel and QIR level of 3. Our results suggest that UHR images using higher levels of QIR with sharper kernel settings could improve distal vessel visualization by increasing spatial resolution while maintaining good image quality.

The improved spatial resolution of the PCCT detector has the potential to radically improve stent assessment, allowing for more accurate detection of in-stent restenosis. Blooming artifact is the main limiting factor that precludes accurate diagnosis of in-stent restenosis on coronary CTA. Therefore, an optimal combination of sharper kernels and noise reduction is needed to achieve the highest diagnostic confidence in evaluating intrastent patency. The difference between the attenuation measured in the stent lumen and coronary lumen adjacent to the stent (ΔHU_{stent}) decreased with increasing QIR levels, with a sharper kernel and with larger slice thickness indicating less pronounced stent induced artifacts. Notably, the combination of 0.2 mm thickness, Bv56 kernel and QIR level 4 was optimal for stents based both on ΔHU_{stent} value and on qualitative analysis. Prior studies showed improved evaluation of both phantom and in vivo coronary stents comparing EID-CT and PCCT using a CT scanner of a different vendor compared to our data [11,12]. Mergen et al also demonstrated that the high temporal resolution of 66 ms provided by the dual source technology is needed to fully exploit the capabilities of UHR scanning [17]. Decker et al. demonstrated that using UHR mode with a 0.2 mm slice thickness and using sharp reconstruction kernels improved the assessment of small stents in a phantom model [18]. Similarly, Geering et al. found that UHR images yielded excellent quality for the evaluation of coronary stents based on 22 patients' data [15]. Further studies are warranted to define the diagnostic accuracy of PCCT using UHR (also labelled Cardiac High Definition [HD] mode), particularly for smaller stent diameters (<3 mm). Our findings can facilitate the adoption of novel PCCT technique by offering the optimal parameters for performing coronary CTA.

5. Limitations

We acknowledge the limitations of our study. Using different virtual monoenergetic images - the standard reconstruction method for 0.4 mm

reconstruction - has also substantial effects on intravascular attenuation and noise parameters, although this has been evaluated in our previous study and also has been demonstrated by other groups [19–21]. Currently there is no unified recommendation for selecting the kernel, slice thickness, and QIR combination for a given patient, therefore large variety exists in coronary CTA protocols. Our selection reflects our current clinical practice which aligns well with the protocol of many other sites using the first generation PCCT scanner and former vendor recommendations. Prior studies suggest even sharper kernels for evaluating UHR images, however the higher BMI seen in our population could limit the use of Bv64 or higher kernels [6–8,22]. Although the use of Bv60 or Bv64 versus Bv56 increases sharpness and reduces blooming, it also substantially reduces CNR (25 % and 35 % decrease) [6] Moreover, FOV and matrix size can also change the assessed metrics, which were kept constant in our current study. Although our study analyzed a relatively small group of patients, it was still able to reliably capture the effect of different reconstruction settings and was larger than previous patient studies [6]. The current study did not assess coronary stenosis using different reconstructions, and no invasive coronary angiography (ICA) was available as a gold standard. Further studies are warranted to define the optimal reconstruction settings for non-calcified and calcified plaque components.

6. Conclusions

Photon-counting CT demonstrated high qualitative and quantitative image quality for the assessment of coronaries and stents. When utilizing the UHR mode along with a high level of QIR, CNR values remained consistent in the distal segments compared to the proximal segments. Our comprehensive evaluation, incorporating both quantitative and qualitative analyses of image quality, revealed distinct reconstruction settings optimized for coronary assessment. According to our qualitative assessment, the highest image quality was found on images with Bv44 kernel, QIR 3/4 and both 0.4 and 0.6 mm on standard images, while Bv56, QIR 4 and 0.2 mm on UHR images.

Twitter Handle: Photon-counting CT using quantum iterative reconstruction offers excellent qualitative and quantitative image quality for the evaluation of coronary arteries and stents. #PCCT #YesCCT.

CRediT authorship contribution statement

Borbála Vattay: Writing – original draft, Visualization, Project administration, Methodology, Investigation, Formal analysis, Data curation. **Melinda Boussoussou:** Investigation, Data curation. **Milán Vecsey-Nagy:** Writing – review & editing, Project administration. **Márton Kolossváry:** Writing – review & editing, Validation, Methodology. **Dénes Juhász:** Project administration, Investigation, Data curation. **Nóra Kerkovits:** Project administration, Investigation. **Hanna Balogh:** Project administration, Investigation. **Norbert Nagy:** Project administration, Investigation. **Miklós Vértes:** Writing – review & editing, Project administration, Investigation. **Máté Kiss:** Writing – review & editing, Supervision. **Anikó Kubovje:** Project administration, Investigation, Data curation. **Béla Merkely:** Resources. **Pál Maurovich Horvat:** Validation, Resources. **Bálint Szilveszter:** Writing – original draft, Visualization, Validation, Supervision, Project administration, Methodology, Investigation, Formal analysis, Conceptualization.

Declaration of competing interest

The authors declare that they have no known competing financial interests or personal relationships that could have appeared to influence the work reported in this paper.

Acknowledgments

Project no. RRF-2.3.1-21-2022-00003 has been implemented with the support provided by the European Union. BV was supported by the ÚNKP-22-3-II-SE New National Excellence Program of the Ministry for Culture and Innovation from the source of the National Research, Development and Innovation Fund. This project was supported by the János Bolyai Research Scholarship of the Hungarian Academy of Sciences. BS was supported by the ÚNKP-23-5 New National Excellence Program of the Ministry for Culture and Innovation from the source of the National Research, Development and Innovation Fund.

Appendix A. Supplementary data

Supplementary data to this article can be found online at https://doi.org/10.1016/j.ejrad.2024.111426.

References

[1] J. Knuuti, W. Wijns, A. Saraste, D. Capodanno, E. Barbato, C. Funck-Brentano, E. Prescott, R.F. Storey, C. Deaton, T. Cuisset, S. Agewall, K. Dickstein, T. Edvardsen, J. Escaned, B.J. Gersh, P. Svitil, M. Gilard, D. Hasdai, R. Hatala, F. Mahfoud, J. Masip, C. Muneretto, M. Valgimigli, S. Achenbach, J.J. Bax, E.S.C.S.D. Group, 2019 ESC Guidelines for the diagnosis and management of chronic coronary syndromes: The Task Force for the diagnosis and management of chronic coronary syndromes of the European Society of Cardiology (ESC), European Heart Journal 41(3) (2019) 407-477.

[2] G. Pontone, A. Rossi, M. Guglielmo, M.R. Dweck, O. Gaemperli, K. Nieman, F. Pugliese, P. Maurovich-Horvat, A. Gimelli, B. Cosyns, S. Achenbach, Clinical applications of cardiac computed tomography: a consensus paper of the european Association of Cardiovascular Imaging-part I, Eur Heart J Cardiovasc Imaging. 23 (3) (2022) 299–314.

[3] T. Flohr, M. Petersilka, A. Henning, S. Ulzheimer, J. Ferda, B. Schmidt, Photon-counting CT review, Phys Med. 79 (2020) 126–136.

[4] M.J. Willemink, M. Persson, A. Pourmorteza, N.J. Pelc, D. Fleischmann, Photon-counting CT: technical principles and clinical prospects, Radiology. 289 (2) (2018) 293–312.

[5] K. Rajendran, M. Petersilka, A. Henning, E. Shanblatt, J. Marsh Jr., J. Thorne, B. Schmidt, T. Flohr, J. Fletcher, C. McCollough, S. Leng, Full field-of-view, high-resolution, photon-counting detector CT: technical assessment and initial patient experience, Phys Med Biol. 66 (20) (2021).

[6] V. Mergen, T. Sartoretti, M. Baer-Beck, B. Schmidt, M. Petersilka, J.E. Wildberger, A. Euler, M. Eberhard, H. Alkadhi, Ultra-high-resolution Coronary CT angiography with photon-counting detector CT: feasibility and image Characterization, Invest Radiol. 57 (12) (2022) 780–788.

[7] J. Greffier, S.A. Si-Mohamed, H. Lacombe, J. Labour, D. Djabli, S. Boccalini, M. Varasteh, M. Villien, Y. Yagil, K. Erhard, L. Boussel, J.P. Beregi, P.C. Douek, Virtual monochromatic images for coronary artery imaging with a spectral photon-counting CT in comparison to dual-layer CT systems: a phantom and a preliminary human study, Eur Radiol. 33 (8) (2023) 5476–5488.

[8] J. von Spiczak, M. Mannil, B. Peters, T. Hickethier, M. Baer, A. Henning, B. Schmidt, T. Flohr, R. Manka, D. Maintz, H. Alkadhi, Photon counting computed tomography with dedicated Sharp convolution kernels: tapping the potential of a new Technology for Stent Imaging, Invest Radiol. 53 (8) (2018) 486–494.

[9] S. Abbara, P. Blanke, C.D. Maroules, M. Cheezum, A.D. Choi, B.K. Han, M. Marwan, C. Naoum, B.L. Norgaard, R. Rubinshtein, P. Schoenhagen, T. Villines, J. Leipsic, SCCT guidelines for the performance and acquisition of coronary computed tomographic angiography: a report of the society of Cardiovascular computed tomography guidelines committee: endorsed by the north American Society for Cardiovascular Imaging (NASCI), J Cardiovasc Comput Tomogr. 10 (6) (2016) 435–449.

[10] J. Karady, A. Panajotu, M. Kolossvary, B. Szilveszter, A.L. Jermendy, A. Bartykowszki, M. Karolyi, C. Celeng, B. Merkely, P. Maurovich-Horvat, The effect of four-phasic versus three-phasic contrast media injection protocols on extravasation rate in coronary CT angiography: a randomized controlled trial, Eur Radiol. 27 (11) (2017) 4538–4543.

[11] G. Bratke, T. Hickethier, D. Bar-Ness, A.C. Bunck, D. Maintz, G. Pahn, P. Coulon, S. Si-Mohamed, P. Douek, M. Sigovan, Spectral photon-counting computed tomography for Coronary stent imaging: evaluation of the potential clinical impact for the delineation of in-stent restenosis, Invest Radiol. 55 (2) (2020) 61–67.

[12] S. Boccalini, S.A. Si-Mohamed, H. Lacombe, A. Diaw, M. Varasteh, P.A. Rodesch, M. Villien, M. Sigovan, R. Dessouky, P. Coulon, Y. Yagil, E. Lahoud, K. Erhard, G. Rioufol, G. Finet, E. Bonnefoy-Cudraz, C. Bergerot, L. Boussel, P.C. Douek, First in-human results of computed tomography angiography for Coronary stent assessment with a spectral photon counting computed tomography, Invest Radiol. 57 (4) (2022) 212–221.

[13] K. Rajendran, M. Petersilka, A. Henning, E.R. Shanblatt, B. Schmidt, T.G. Flohr, A. Ferrero, F. Baffour, F.E. Diehn, L. Yu, P. Rajiah, J.G. Fletcher, S. Leng, C. H. McCollough, First clinical photon-counting detector CT system: technical evaluation, Radiology. 303 (1) (2022) 130–138.

[14] M. Soschynski, F. Hagen, S. Baumann, M.T. Hagar, J. Weiss, T. Krauss, C.L. Schlett, C. von Zur Muhlen, F. Bamberg, K. Nikolaou, S. Greulich, M.F. Froelich, P. Riffel, D. Overhoff, T. Papavassiliu, S.O. Schoenberg, S. Faby, S. Ulzheimer, I. Ayx, P. Krumm, High temporal resolution dual-source photon-counting CT for Coronary artery disease: initial multicenter clinical Experience, J Clin Med. 11 (20) (2022).

[15] L. Geering, T. Sartoretti, V. Mergen, G. Cundari, S. Rusek, F. Civaia, P. Rossi, J. E. Wildberger, C. Templin, R. Manka, M. Eberhard, H. Alkadhi, First in-vivo coronary stent imaging with clinical ultra high resolution photon-counting CT, J Cardiovasc Comput Tomogr. 17 (3) (2023) 233–235.

[16] M. Vecsey-Nagy, A. Varga-Szemes, T. Emrich, E. Zsarnoczay, N. Nagy, N. Fink, B. Schmidt, T. Nowak, M. Kiss, B. Vattay, M. Boussoussou, M. Kolossvary, A. Kubovje, B. Merkely, P. Maurovich-Horvat, B. Szilveszter, Calcium scoring on coronary computed angiography tomography with photon-counting detector technology: Predictors of performance, J Cardiovasc Comput Tomogr (2023).

[17] V. Mergen, T. Sartoretti, G. Cundari, M. Serifovic, K. Higashigaito, T. Allmendinger, B. Schmidt, T. Flohr, R. Manka, M. Eberhard, H. Alkadhi, The importance of temporal resolution for ultra-high-resolution Coronary angiography: evidence from photon-counting detector CT, Invest Radiol. (2023).

[18] J.A. Decker, J. O'Doherty, U.J. Schoepf, T.M. Todoran, G.J. Aquino, V. Brandt, D. Baruah, N. Fink, E. Zsarnoczay, T. Flohr, B. Schmidt, T. Allmendinger, F. Risch, A. Varga-Szemes, T. Emrich, Stent imaging on a clinical dual-source photon-counting detector CT system-impact of luminal attenuation and sharp kernels on lumen visibility, Eur Radiol. 33 (4) (2023) 2469–2477.

[19] B. Vattay, B. Szilveszter, M. Boussoussou, M. Vecsey-Nagy, A. Lin, G. Konkoly, A. Kubovje, F. Schwarz, B. Merkely, P. Maurovich-Horvat, M.C. Williams, D. Dey, M. Kolossvary, Impact of virtual monoenergetic levels on coronary plaque volume components using photon-counting computed tomography, Eur Radiol. (2023).

[20] T. Sartoretti, M. McDermott, V. Mergen, A. Euler, B. Schmidt, G. Jost, J. E. Wildberger, H. Alkadhi, Photon-counting detector coronary CT angiography: impact of virtual monoenergetic imaging and iterative reconstruction on image quality, Br J Radiol. 96 (1143) (2023) 20220466.

[21] D. Pinos, J. Griffith 3rd, T. Emrich, U.J. Schoepf, J. O'Doherty, E. Zsarnoczay, N. Fink, M. Vecsey-Nagy, P. Suranyi, C. Tesche, G.J. Aquino, A. Varga-Szemes, V. Brandt, Intra-individual comparison of image quality of the coronary arteries between photon-counting detector and energy-integrating detector CT systems, Eur J Radiol. 166 (2023) 111008.

[22] Emily K. Koons, Prabhakar Shantha Rajiah, Jamison E. Thorne, Nikkole M. Weber, Holly J. Kasten, Elisabeth R. Shanblatt, Cynthia H. McCollough, Shuai Leng, Coronary artery stenosis quantification in patients with dense calcifications using ultra-high-resolution photon-counting-detector computed tomography, Journal of Cardiovascular Computed Tomography, ISSN 1934-5925 (2023) 10.1016/j.jcct.2023.10.009.